ceramics

MDPI

Article

Influence of the Feedstock Preparation on the Properties of Highly Filled Alumina Green-Body and Sintered Parts Produced by Fused Deposition of Ceramic

Thomas Heim * and Frank Kern

Institute for Manufacturing Technologies of Ceramic Components and Composites (IFKB), University of Stuttgart, Allmandring 7B, 70569 Stuttgart, Germany

* Correspondence: thomas.heim@ifkb.uni-stuttgart.de

Abstract: This paper investigates new approaches for the blending and plastification of ceramic powder with a binder to form fused deposition of ceramic (FDC) feedstock. The fabrication of highly filled ceramic filaments was accomplished using the granulation by agitation technique, followed by twin-screw extruder homogenization and single-screw extruder filament extrusion. The feedstocks are based on alumina (Al_2O_3) powders, which were prepared with an industrial binder through three different routes: wet granulation, melt granulation and melt granulation with a suspension. After printing cubic samples and tensile test specimens on a commercial fused deposition modelling (FDM) printer, the properties of the resulting green-body and sintered parts were investigated. The green-body mechanical values are compared with results from commercially available filaments. Mixing the binder with the alumina powder and surfactant in a suspension produces the lowest viscosity and the best elongation at break.

Keywords: feedstock preparation; fused deposition of ceramic; properties of ceramic green-body; alumina filament; ceramic additive manufacturing

Citation: Heim, T.; Kern, F. Influence of the Feedstock Preparation on the Properties of Highly Filled Alumina Green-Body and Sintered Parts Produced by Fused Deposition of Ceramic. *Ceramics* **2023**, *6*, 241–254. https://doi.org/10.3390/ceramics6010014

Academic Editor: Gilbert Fantozzi

Received: 30 November 2022
Revised: 24 December 2022
Accepted: 5 January 2023
Published: 11 January 2023

1. Introduction

Most of the additive manufacturing processes have been adapted to ceramic materials [1]. Fused deposition modelling (FDM) is a wide-spread technique for professional and household applications [2,3]. Despite many technological advances [4], the field of applications for its ceramic counterpart, fused deposition of ceramic, remains much narrower than polymer or metal fused filament fabrication (FFF) [1]. One explanation comes from the sensitivity of ceramic materials towards specific defects inherent in the material extrusion-based additive manufacturing (MEAM) processes: the staircase effect, limited precision and the greater susceptibility to pore formation. These defects not only deteriorate the esthetic aspect of the parts, they also lower the fracture strength of the ceramic component [5,6] through stress concentration and crack initiation [7].

Similar to ceramic injection molding (CIM) the polymeric material in FDC is only used as a means for the forming process. It is then removed with catalytical, solvent and/or thermal debinding [8]. The goal for a good feedstock is a high-volume fraction of solid content and a good flowability [9,10]. This high solid content should be well distributed among the feedstock from the mixing step [11] because inhomogeneity in the filament leads to pore formation, irregular sintering shrinkage and, in the end, to deficient parts.

Alumina is the most important technical oxide ceramic and has a broad field of applications [7]. The alumina powder used in this study was already successfully processed for FDC application [10,12].

Many publications on the FDC process focus on the selection of appropriate binder compositions [8,13], whereas in CIM, the importance of binder preparation on the properties of the feedstock is documented [9,14,15]. In order to minimize the defect occurrence and to

obtain a flawless sintering shrinkage, the homogeneous distribution of the powder in the binder is of primary importance. Agglomerated particles influence not only the rheological properties of the ceramic mixtures but also the critical powder volume concentration of a feedstock [11], the sintering process and, in the end, the mechanical properties of the sintered ceramics [15]. These agglomerates may not be totally destroyed in the mixing steps [15]. Dispersing the ceramic powder before blending it with a binder may solve the issues caused by agglomerates. Furthermore, the preparation of feedstock with a mixer granulator can reduce the preparation time for highly filled ceramic feedstock [9].

However, in contrast to CIM, the green-body property of the filament in FDC plays a crucial role in the reliability of the process. Brittle filaments are constraining as they require modified printers or manual feeding [16,17]. Filament rupture may not only cause a loss of time but also irregular extrusion rates and irregular cooling if the printing process needs to be stopped. Therefore, not only the properties of the sintered parts but also the mechanical properties of the filament should be considered for improving the material and process.

This work aims to present the influence of the feedstock preparation on the rheological and mechanical properties of the filament and green-body, as well as their effects on the sintered parts.

2. Materials and Methods

2.1. Materials

A fine high-purity alumina CT 3000 LS SG (Almatis GmbH, Frankfurt, Germany) was used in this study. The industrial binder Kcmix® 3.3 (KRAHN Ceramics GmbH, Hamburg, Germany) was used for compounding. Then, 800 g alumina powder and 200 g of polymer pellets were dosed gravimetrically, which provided a mass ratio of 80% ceramic powder to 20% binder.

In one of the filament compositions (cf. Section 2.2 below), Dolapix CE 64 (Zschimmer and Schwarz GmbH and Co. KG, Lahnstein, Germany), a dispersing additive was added. This suspension was deagglomerated with 2 mm alumina beads in a rotating container for 10 h. Particle size distribution (PSD) was measured using a laser granulometer Mastersizer 3000 with the Hydro LV wet sample dispersion unit (Malvern Panalytical, Malvern, UK). The raw and the deagglomerated ceramic powders were dispersed in distilled water and added into the water-based measuring cell until the obscuration level reached approximately 15%. The assumed refractive index for particle size calculations according to the Mie model was 1.76 for Al_2O_3.

To compare the green-body properties, two commercial alumina filaments with unknown compositions from Zetamix (Nanoe, Ballainvilliers, France) and SiCeram (SiCeram GmbH, Jena, Germany) were used.

2.2. Filament Preparation

The filaments were manufactured according to the process illustrated in Figure 1.

For blending and plastification, an Eirich R02 mixer (Maschinenfabrik Gustav Eirich, Hardheim, Germany) was used.

The first variant, further denominated V1, was prepared through wet granulation. The ceramic powder was mixed with the binder's pellets, and 100 mL water was added in 25 mL steps until the powder agglomerated around the pellets and granulates were formed.

The second variant, further denominated V2, was processed by melt-granulation. The binder was first melted in the Eirich mixer. When the temperature reached 135 °C, the ceramic powder was added. The feedstock was continuously stirred and the temperature was increased until 160 °C was attained. Then, the feedstock was quickly cooled down by adding 400 mL water in 50 mL steps until the right granule size was reached.

For the third variant, further denominated V3, the same procedure as V2 was used. The difference was in the fact that the ceramic powder was added in form of a suspension and heated up with the binder until the water fully evaporated. The suspension was composed by the ceramic powder, dispersed with 15.1 g Dolapix CE 64 surfactant in

538 g water. This suspension was previously deagglomerated with 2 mm alumina beads in a rotating container for 10 h.

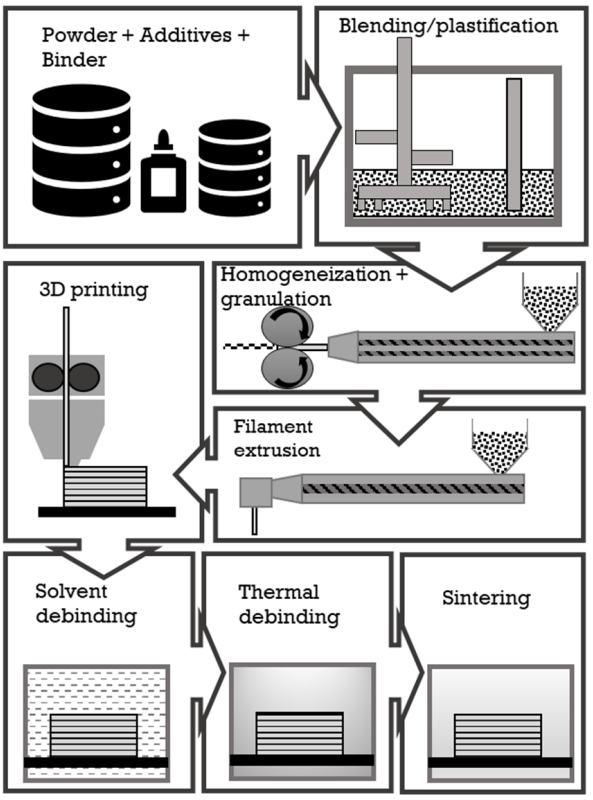

Figure 1. Schematic representation of the process.

After the granulation, all the feedstocks were dried in an oven at 40 °C for 48 h.

The feedstock was then homogenized three times through a twin-screw extruder (HAAKE Polylab OS Rheomex PTW16/25 OS, Thermo Fisher Scientific, Karlsruhe, Germany) with the temperature settings for the segments ranging from 85 °C to 135 °C.

A single screw extruder (HAAKE Polylab OS Rheomex 19/10 OS, Thermo Fisher Scientific, Karlsruhe, Germany) was used to produce the 1.75 mm diameter filaments combined with an in-house filament cooling and pulling machine (cf. Figure 2) with an integrated regulation system through an ODAC 14XY laser diameter sensor (Zumbach Electronic GmbH, Pulheim, Germany). The segment temperatures of the extruder were set between 100 and 130 °C.

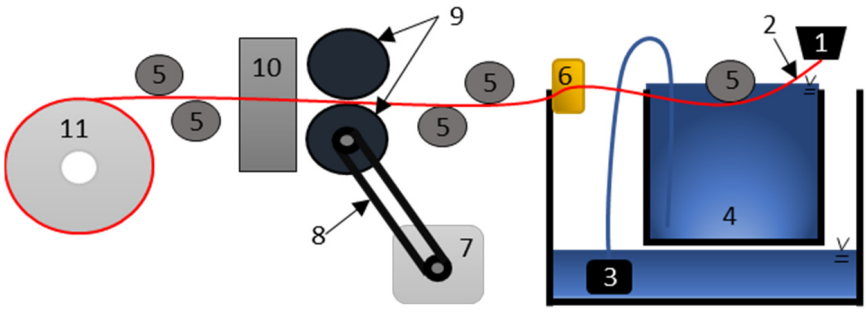

Figure 2. Schematic representation of the filament pulling machine. 1: nozzle of the single-screw extruder, 2: filament, 3: water pump, 4: water container, 5: guide wheel, 6: sponge, 7: stepper motor, 8: timing belt transmission, 9: PU rubber conveyor wheel, 10: laser measuring head, 11: filament spool.

The continuous diameter measurements of at least 8 m of the extruded filament were effectuated with the ODAC 14XY laser diameter sensor. The measuring head comprises two sensors positioned with a 90° rotation. The roundness in millimeter (mm) of the filament is calculated as follows for each measurement:

$$\frac{(\text{maximum diameter}) - (\text{minimum diameter})}{2} \quad (1)$$

2.3. 3D Printing

The cubic specimens with a 15 mm edge length were sliced on the Slic3r 2.3.0 software (Prusa Research, Praha, Czech Republic) with two outer layers and a linear infill pattern with 90° change between each layer. The tensile test specimens were also sliced with two outer layers, but the infill pattern was linear and aligned in the direction of loading.

All the test samples were printed on a i3 MK3 from Prusa with a flexible steel sheet print bed (Prusa Research, Praha, Czech Republic) that was converted for printing ceramics by replacing the nozzle with a specific wear-resistant nozzle from Gühring (Gühring KG, Albstadt, Germany) to guarantee a stable feed rate and a stable diameter due to limited abrasion. After printing, the samples were maintained in normal conditions at 23 °C and with a relative humidity of 20%. The printing parameters for the V1, V2, and V3 filaments can be seen in Table 1.

Table 1. Filament printing parameters.

Nozzle diameter	0.6 mm
Layer height	0.15 mm
Layer thickness	0.65 mm
Printing speed	25 mm/s
Fan speed	100%
Infill	100%
Flow	100%
Printing temperature	135 °C

The printing temperatures of the SiCeram and Zetamix filaments were, respectively, 165 °C and 110 °C according to the suppliers' recommendations.

2.4. Debinding

In the first solvent debinding step, the parts were dipped into acetone at 40 °C for at least 12 h until the mass loss reached at least 6 wt.% to create an open porosity for the thermal debinding. The second debinding step is based on a temperature program presented in the work of Sommer [18] and can be seen in Figure 3.

2.5. Sintering

The parts were sintered in a HT Speed sintering oven (Mihm-Vogt GmbH and Co. KG, Stutensee-Blankenloch, Germany) at a temperature of 1550 °C for 120 min with a heating rate of 1 K/min and a cooling rate of 2 K/min. In the sintering oven, the parts were positioned the same way as on the printing plate.

2.6. SEM

The SEM micrographs were taken on a JSM-6490 (JEOL, Freising, Germany). The samples were embedded, ground for the filaments' samples, and polished for the sintered samples. After polishing, the sintered samples were thermally etched for 10 min at 1300 °C with a heating rate of 10 K/min.

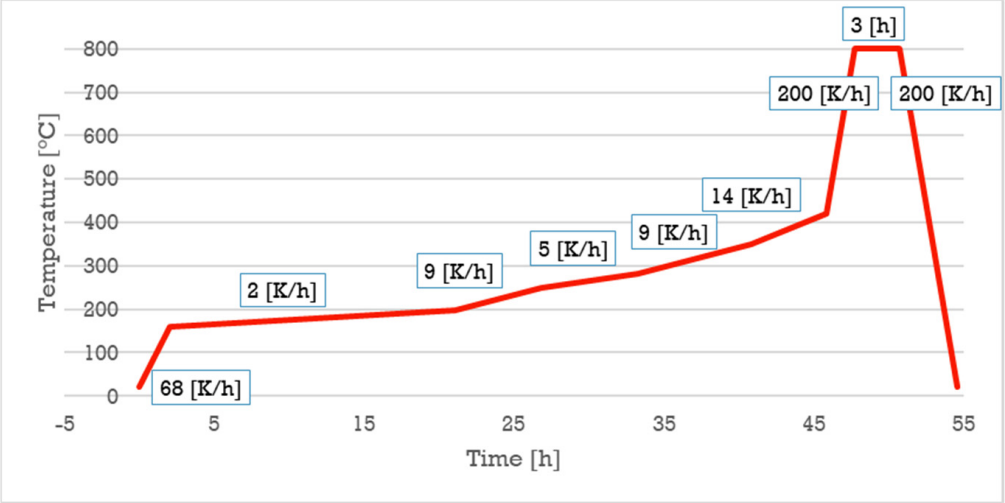

Figure 3. Time–temperature debinding program.

2.7. Properties of Green-Bodies

2.7.1. Density of the Green-Bodies

The apparent density was measured with the Archimedes method. Six printed cubic samples for each filament were tested. The water temperature was 21.7 °C, which corresponded to a water density of 997.8 $\frac{kg}{m^3}$.

2.7.2. Tensile Test

The tensile test of the 3D printed green-body was performed according to the EN ISO 527-2:2012 specifications on three 1BA 3D printed specimens (cf. Figure 4).

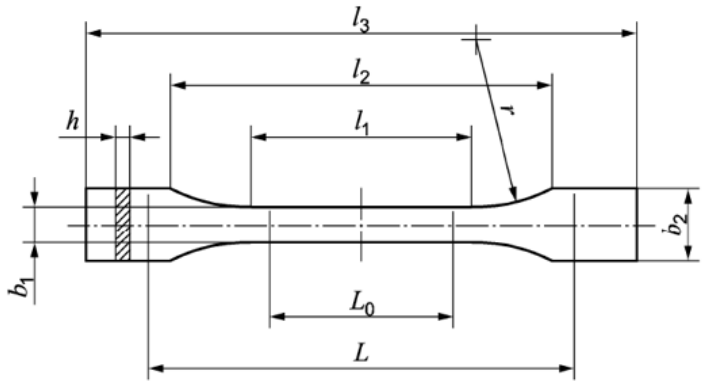

1BA	[mm]
l3	≥ 75
l1	30 ± 0.5
r	≥ 30
l2	58 ± 2
b2	10 ± 0.5
b1	5 ± 0.5
h	≥ 2
L0	25 ± 0.5
L	$l2_0^{+2}$

Figure 4. Geometry and dimensions of 1BA EN ISO 527-2:2012 tensile test specimen [19].

The testing machine used was a universal Zwick Z100 (Zwick GmbH and Co. KG, Ulm, Germany) with a crosshead speed of 1 mm/min. The samples were tested in a room at 23 °C with 20% relative humidity. The ultimate tensile strength (2), the elongation at break (3) and the Young's modulus (4) of the composite tensile specimens were calculated as follows:

$$\sigma_m = F_{max}/A \quad (2)$$

$$\varepsilon_b = L_b/L \quad (3)$$

$$E_t = d\sigma/d\varepsilon \quad (4)$$

where, σ_m is the ultimate tensile strength in Megapascals (MPa), F_{max} is the maximum force measured during the tensile test in Newtons (N), A is the theoretical initial cross-section in square millimeters (mm^2), ε_b is the strain at break in percentage (%), L_b is the length of the part between the grips at which the strength is smaller than 0.9 σ_m and is given in millimeters (mm), L is the initial length of the part of the specimen between the grips as defined by EN ISO 527-2:2012 in millimeters (mm), E_t is the tensile modulus in Gigapascals (GPa), and $d\sigma/d\varepsilon$ is the slope of the regression curve in Gigapascals (GPa).

Young's modulus of the composite tensile specimens was defined by the slope of the least-squares' regression of the stress/strain curve between 0.05% and 0.25% strain according to the norm.

2.7.3. Rheology

The rheology was measured through frequency-sweep on a Discovery HR-2 rheometer (TA Instruments, New Castle, DE, USA) at 145 °C with an oscillation strain of 0.1%.

2.8. Properties of Sintered Parts

2.8.1. Sintering Shrinkage

The sintering shrinkage was measured on three cubic samples for each feedstock's variant with a green-body edge length of 15 mm, except for the V2 samples, where it could only be measured on one sample because of the delamination during the debinding of the two other samples. The measurements were taken in the middle line of the sides with an Orion electronic caliper (HAHN+KOLB Werkzeuge GmbH, Ludwigsburg, Germany). Each printing direction was considered. The sintering shrinkage, given in percentage (%), was calculated as follow

$$\frac{Ls - L0}{L0} \tag{5}$$

where Ls and $L0$ are, respectively, the edge length of the sintered part and the green-body in millimeters (mm).

2.8.2. Density of the Sintered Samples

The density was measured according to the EN ISO 18754:2022 norm with impregnation of the test pieces in vacuum. The same cubic samples as for the sintering shrinkage measurements were tested. The water temperature was 22.3 °C, which corresponded to a water density of 997.7 $\frac{kg}{m^3}$. The theoretical density of the alumina considered for the calculation of the relative bulk density was 3.95 $\frac{kg}{m^3}$

2.8.3. Hardness

Vickers hardness HV10 measurements (Bareiss Prüfgerätebau GmbH, Oberdischingen, Germany) were performed with a 10 kgf load applied for ten seconds on one polished sample for each feedstock variant. The resulting Vickers hardness represents the mean of five measurements.

2.8.4. E-Modulus

Since for isotropic materials, the indentation modulus should be equal to the Young's modulus, the obtained values were used as Young's modulus for further calculations [20]. The micro indentation modulus measurement was performed on a Fischerscope® HM2000 (Helmut Fischer GmbH, Sindelfingen, Germany) with the universal hardness method. Six measurements were taken for each sample, randomly distributed on the surface.

2.8.5. Toughness

The Vickers indentation fracture toughness was used to determine the fracture toughness of the printed materials using the equation given by Niihara for median cracks ($c/a > 2.5$) [21]:

$$\left(\frac{K_{C(HV)}\varphi}{Ha^{\frac{1}{2}}}\right)\left(\frac{H}{E\varphi}\right)^{\frac{2}{5}} = 0.129\left(\frac{c}{a}\right)^{-\frac{3}{2}} \quad (6)$$

where $K_{C(HV)}$ is the critical stress intensity factor in [MPa$\sqrt{}$m], φ is the constrain factor, H is the Vickers hardness in [MPa], E is the Young's modulus in [MPa], c is the radial crack size in [m], a is the indent half-diagonal in [m].

3. Results

3.1. Filament Preparation

The effect of the deagglomeration and the dispersion of the powder on the particle size distribution can be seen in Figure 5. Medium and big agglomerates break down to form the fine ceramic dispersion used for the V3 filament version.

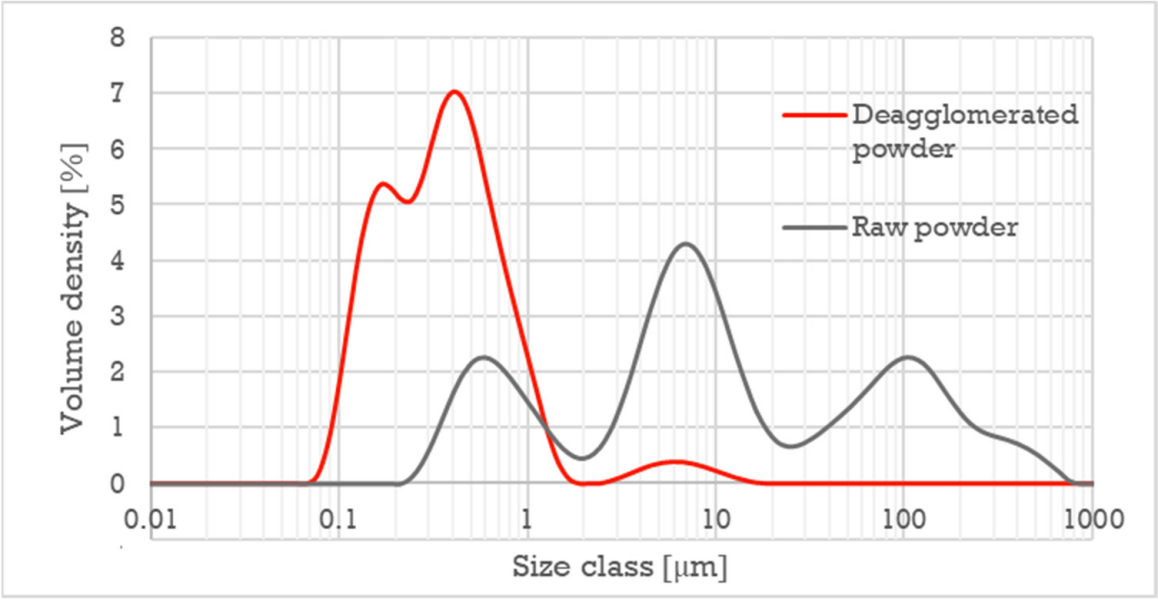

Figure 5. Particle size distribution of the raw CT 3000 LS SG alumina powder.

After the granulation in the Eirich mixer of the V1 feedstock, the bond between the ceramic powder grains and the binder-pellets is too weak; therefore, there is a risk of separation during the processing caused by the vibrations in the twin-screw extruder's hopper. This effect, which could lead to inhomogeneity of the ceramic content along the filament, could be avoided by adding only small amounts of pellets continuously so that the ratio of powder to binder in the extruder remain constant.

All three preparation processes (V1, V2, V3) were successfully achieved and resulted in filaments with good qualitative characteristics that could be wound on a spool and printed without issues. The manufactured filaments had a mean diameter of 1.69 ± 0.03 mm for the V1 filament, 1.68 ± 0.07 mm for the V2 filament and 1.68 ± 0.04 mm, for the V3 filament, with a roundness of, respectively, 0.05 ± 0.02 mm, 0.02 ± 0.02 mm and 0.03 ± 0.03 mm. SEM micrographs of the V1, V2, V3 filaments presented in Figure 6 show a homogeneous dispersion of the ceramic powder and no signs of porosities.

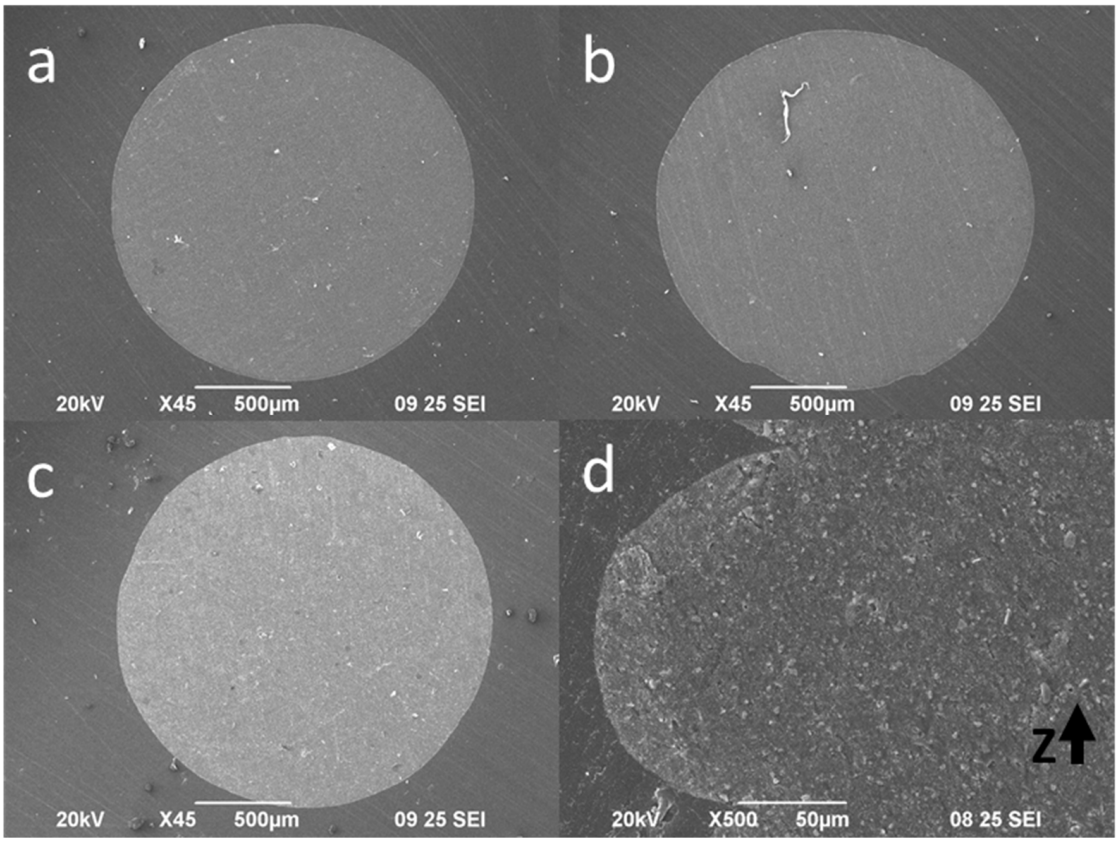

Figure 6. SEM micrographs of the ground cross-sections of the V1 filament (**a**), V2 filament (**b**), V3 filament (**c**) at mag. ×45, and V3 printed cubic sample (**d**) at mag. ×500, Z: vertical printing direction.

3.2. Properties of Green-Bodies

The relatively large nozzle's diameter of 0.6 mm could prevent the clogging during the printing. The V3 printed cubic samples displayed in Figure 6 do not present any major porosity or binder segregation, delamination, texture inside the layers, or visible specific orientation of the grains. As for the filaments, the dispersion of the ceramic powder is homogeneous.

All the filaments were printed successfully. The Zetamix filament tended to break between the spool and the extruder during the printing process. This issue did not appear for the other filaments.

The mass of the six printed cubes was 7.87 ± 0.17 g for the V1 samples, 8.15 ± 0.31 g for the V2 samples, 7.94 ± 0.24 g for the V3 samples, and the apparent density was 2.38 ± 0,03 $\frac{g}{cm^3}$ for the V1 samples, 2.43 ± 0.06 $\frac{g}{cm^3}$ for the V2 samples and 2.38 ± 0.06 $\frac{g}{cm^3}$ for the V3 samples.

The Young's modulus, ultimate tensile strength and the elongation at break of the green-body tensile specimens are displayed in Figure 7. The Young's moduli are higher for the Kc3.3 based filaments than the commercial filaments with, respectively, 484 ± 123 MPa, 606 ± 46 MPa and 436 ± 31 MPa for V1, V2 and V3 samples versus 325 ± 36 MPa and 166 ± 40 MPa for the SiCeram and Zetamix printed samples. Young's modulus and the ultimate tensile strength show similar tendencies.

The elongation at break of the V3 samples and the SiCeram samples with, respectively, 12.1 ± 1% and 14.2 ± 1% exhibited approximately twice the values of the V1 and V2 samples and much higher than the 3.7 ± 0.7% of the Zetamix specimens. It must be specified that most of the tensile specimens broke at the same points just before the junction of the narrow and the broad part of the test specimen, due probably to the printing path defined by the slicer.

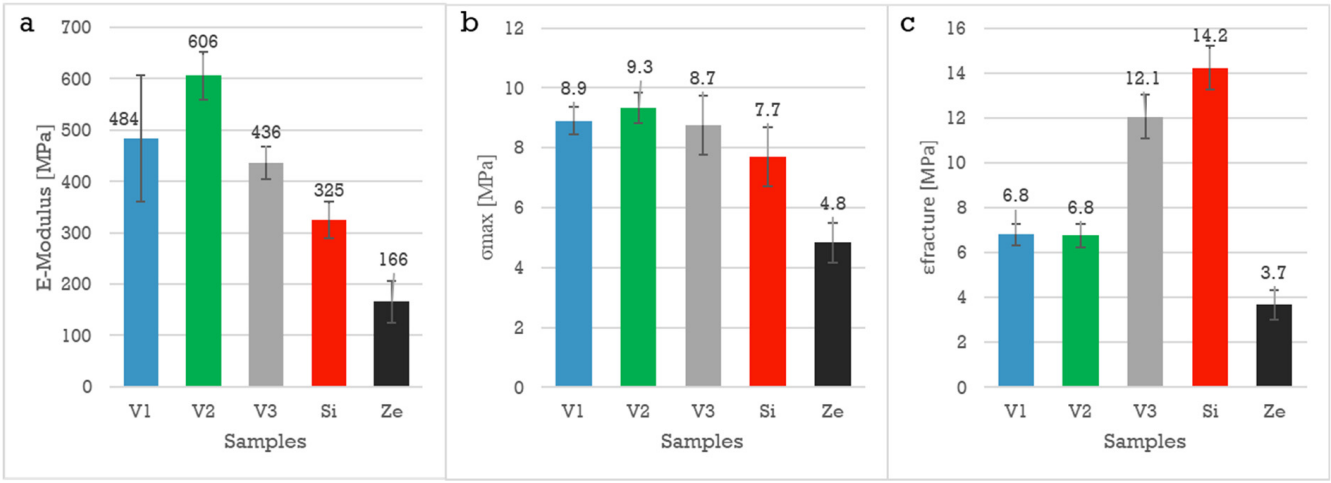

Figure 7. Young's moduli (**a**), ultimate tensile strength (**b**), elongation at break (**c**) of the V1, V2, V3, Si (SiCeram), Ze (Zetamix) printed green-body tensile specimens.

The mean ultimate tensile strength for all the printed tensile specimens, except for the Zetamix, was above 7 MPa, which can be considered a good material strength value for processing the filament with conventional FDM printers in comparison to other highly filled ceramic filaments for FDC applications [13].

The complex viscosity of the V3 feedstock obtained with the ceramic suspension was lower than the viscosity of the V2, and V1 feedstocks (cf. Figure 8). All the filaments presented a shear thinning behavior. The viscosities of the commercial filaments were also measured but were less meaningful since the measurements were taken at 145 °C, which is not the temperature recommended by the suppliers, respectively, 155–170 °C for the SiCeram filament and 110 °C for the Zetamix filament.

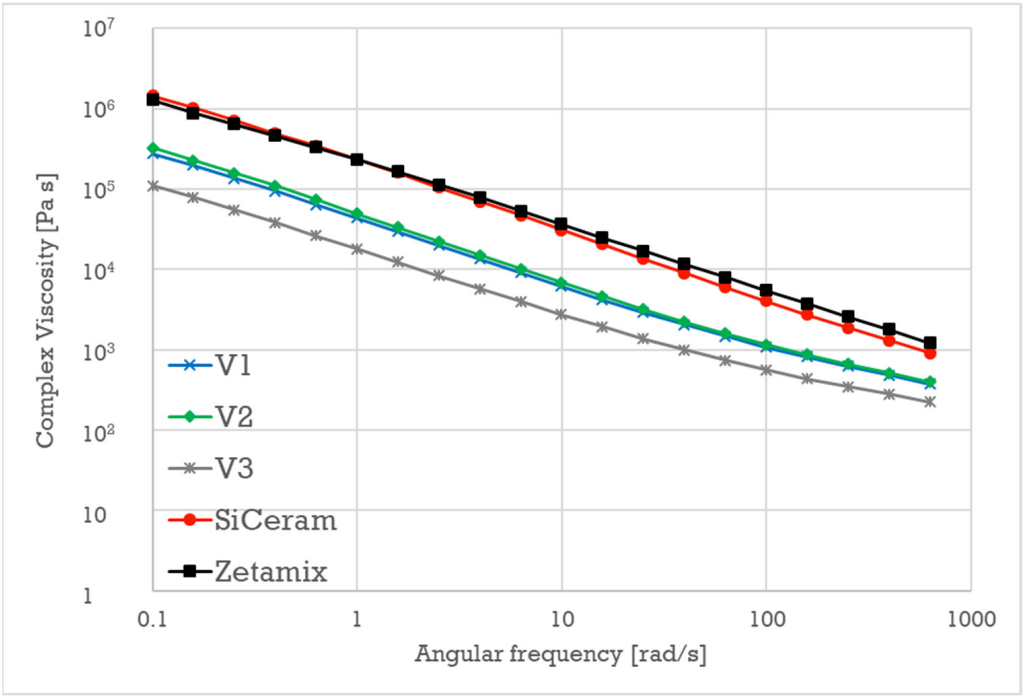

Figure 8. Complex viscosity of the V1, V2, V3, SiCeram and Zetamix filaments at 145 °C.

3.3. Properties of Sintered Parts

The sintering shrinkage exposed in Figure 9 was similar for the three feedstock variants. The shrinkage is anisotropic as it is higher in the z-direction than in the x or y-directions for all the samples. A slight orientation of the grains during extrusion could be the cause, even if Figure 6 and Figure 12 present no apparent texture. The cubic samples being printed with an 0–90° infill pattern, the sintering shrinkage in the x- and z-directions is analogous. The mean sintering shrinkage of the z-axis for the V1 sample is noticeably lower than for the V2 and V3 samples.

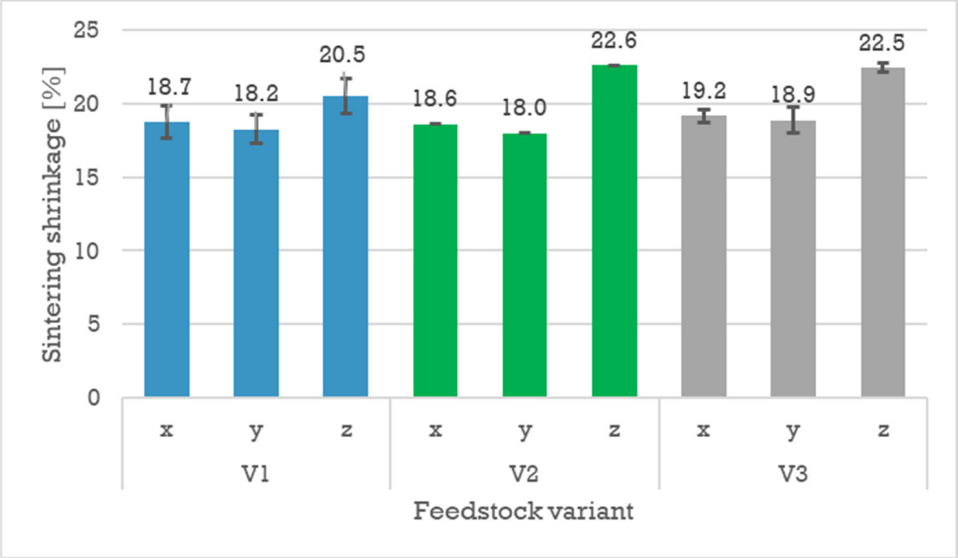

Figure 9. Sintering shrinkage of the V1, V2 and V3 printed cubic samples.

After sintering, the mean bulk density and the apparent porosity of the V1 indicated Figure 10 was slightly higher, but the standard deviations of the measurements were consequent. The 10% relative bulk density missing was consistent with the apparent porosity values, which meant that most of the porosity came from open pores. This open porosity, which was situated between the extruded layers and exhibited the classical triangle shape for the FFF process, could be seen in micrographs not displayed in this paper. The microstructure of the extruded and sintered strands was dense (cf. below Figure 12 of the V3 sample).

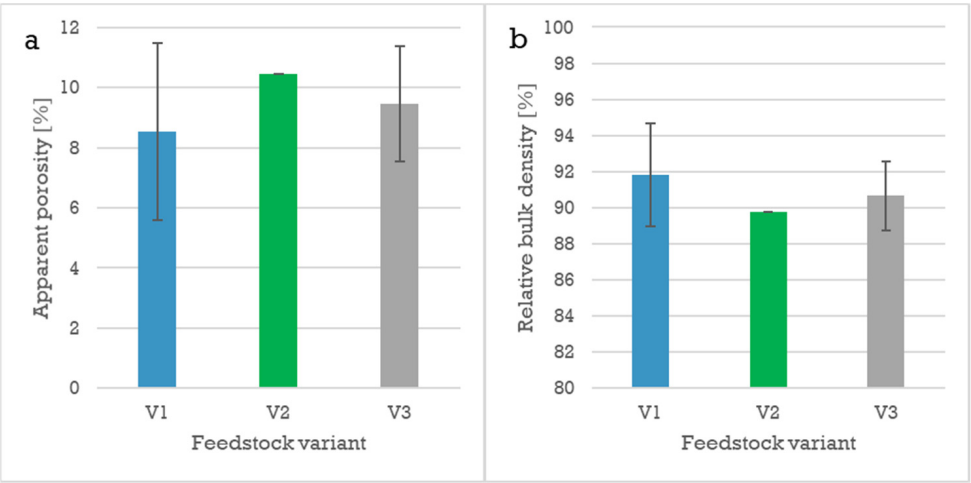

Figure 10. Apparent porosity (**a**), and relative bulk density (**b**) of the V1, V2, V3 sintered samples at 1550 °C for 120 min.

Despite the high open porosity due to printing defects that makes V1, V2, and V3 samples not representative for structural parts, the Young's modulus derived from the indentation modulus, the Vickers's hardness and the fracture toughness, displayed in Figure 11, show expected values for alumina. The indentation modulus and Vickers hardness can be considered identical for the three variants. The fracture toughness determined by indentation presents values between 3 MPa$\sqrt{m}$ and 4 MPa$\sqrt{m}$, which are attributable to the bulk material, since the indentations were made relatively far away for the macro-pores.

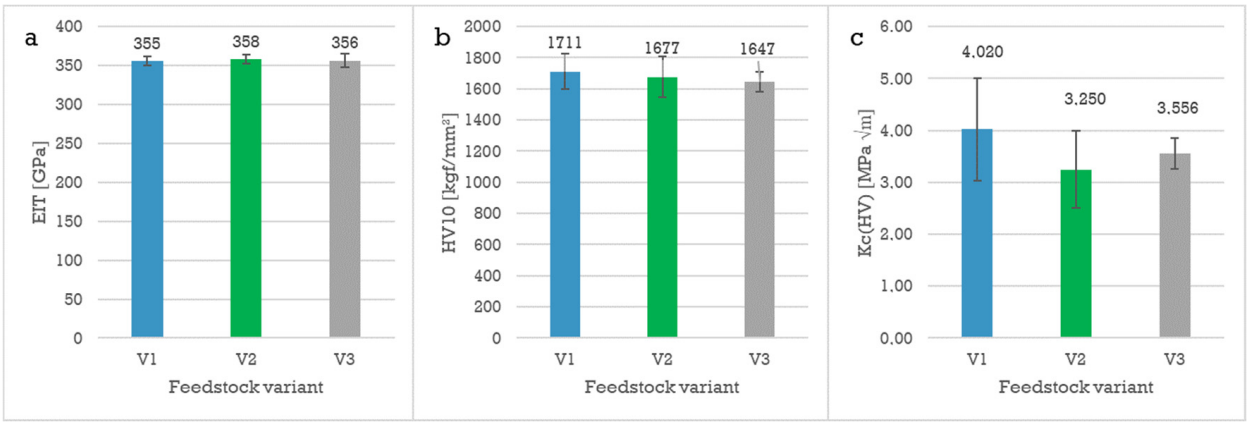

Figure 11. Indentation modulus (**a**), Vickers hardness HV10 (**b**), indentation toughness after Niihara (**c**).

As for the green-body micrograph presented in Figure 6, no visible specific texture of grain orientation is noticeable in the SEM micrographs in Figure 12. The porosity inside the deposited lines is low, but one can recognize elongated pores at the interface between the deposited layers, which remains even if there is grain growth between the layers.

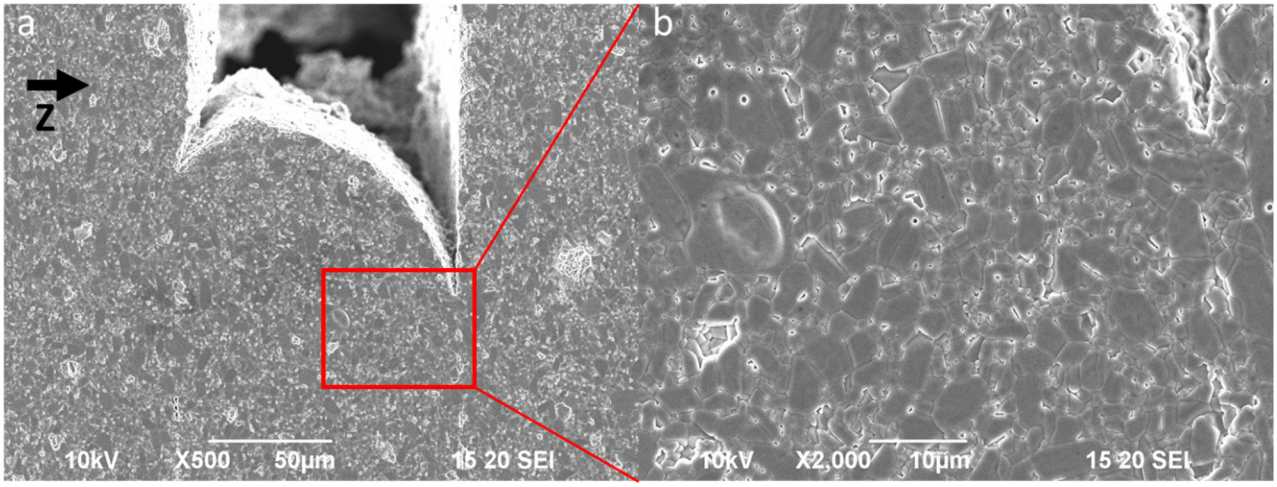

Figure 12. SEM micrographs of the cross-section of a V3 sample after sintering at 1550 °C for 120 min and thermal etching at 1300 °C for 10 min. at mag. ×500 (**a**) and mag. ×2000 (**b**), Z: vertical printing direction.

4. Discussion

The blending step of ceramic with a binder, with the ceramic either in a suspension or as raw powder, influences the mechanical properties and the rheology of an additively manufactured green-body.

Mixing the feedstock from ceramic suspension, as in the V3 path, reduces the viscosity in comparison to the V1 and V2 feedstocks. These results are consistent with the works of Sommer et al. and Trunec et al. on ceramic injection molding [14,15]. The

lower viscosity could be explained by a better dispersion of the ceramic powder and the breaking of small agglomerates, although the larger agglomerates are disintegrated during the homogenization for all feedstock variants [15,22]. The surfactant concentration, up to a certain point, may also be beneficial for the viscosity by building a layer around the particles [12].

Lower viscosity allows a good flow of the extruded feedstock, which in turn, reduces the pressure needed to extrude the filament and the forces in the extruder. This improvement of the rheology means also that it is possible to increase the powder content of the filament before reaching the threshold at which the filament cannot be printed. High forces can cause failures or buckling of the filament, leading to lower quality or printing failures [8,23]. A good flowability of the extruded material allows contact between the deposited strands. Furthermore, the parts can be printed at higher volumetric speeds. For this material and these printing parameters, the difference in viscosity between the filaments does not seem to affect the printing of the samples since the mass and the density of the cubic samples are very similar for the three prepared versions.

In addition to homogeneity and low viscosity, the two important properties to easily print filament are, on the one hand, a high Young's modulus to avoid the buckling of filament inside the extruder and to be able to build high pressures in the nozzle, and on the other hand, high elongation at break to be able to wind the filament around a spool and to avoid ruptures during printing. The FDC filaments and the green-bodies can be considered particle-reinforced composites. The significant difference in mechanical properties between the polymer matrix and the reinforcement particles, especially for the strain, causes important stress concentrations at the interface [24]. The strain localization at a local level caused by the inhomogeneous nucleation of damages leads to partial decohesion and crack propagation to a certain extent [24,25]. To remove the influence of the printing process to better investigate the material properties, it would be better to directly extrude tensile test specimens. The higher elongation at break of the V3 specimens could be explained by either a better coverage of the powder grains by the binder; a better binding due to the surfactant; a better dispersion of the powders, thereby reducing the strain concentration; or a combination of the three aforementioned effects [26]. The difference in Young's modulus between the V1, V2 and V3 samples could be explained by different moisture contents [27]. The samples were not dried before testing, which could have led to uncontrolled moisture intakes. The mechanical properties of the V3 filament are comparable to the Siceram filament but better than the Zetamix filament for the printing process.

A constant filament diameter is a key to a successful FFF with good quality. For a 1.75 mm filament, changing the diameter by 0.1 mm changes the volume by more than 10%. The fixed diameter for the extruded filaments was 1.68 mm in order to avoid the clogging in the extruder caused by possible diameter irregularities. Since the filament diameter was set to 1.75 mm in the slicer, this caused under-extrusion, which led to the high open porosity results. One solution, which was later successfully applied, was to set the extrusion coefficient above 1. The surface quality decreased, but with this technique, it was possible to obtain parts with relative bulk densities higher than 99%.

During the first debinding step in acetone, delamination occurred, especially for the V2 samples. This delamination could be removed in further works by printing at higher temperatures. However, increasing the temperature also decreased the viscosity, which in turn, decreased the precision of the print and the possibility to print overhangs and bridges. At higher temperatures, the binder in the filament also began to decompose.

The anisotropic sintering shrinkage behavior was explained by Conzelmann et al. as the consequence for the alignment in the x–y plane of the irregular-shaped powder grains [10]. Since the powder is not spherical and the melted feedstock experience shear and elongation in the nozzle [28] it is likely to happen. However, no visible specific grain orientation can be seen from the SEM micrographs in Figure 12. This aspect could easily be verified in a further study.

5. Conclusions

In this paper three preparation paths for processing highly filled ceramic filament were successfully investigated. Blending a feedstock from a deagglomerated ceramic suspension with surfactant results in lower viscosity and higher elongation at break in comparison to mixing the binder with unprepared dry ceramic powder. The preparation path shows no influence on the indentation modulus, hardness and indentation toughness of the sintered parts, since the values obtained are analogous for the three developed feedstocks

For all three feedstocks, the porosity was similar and mainly due to the printing parameters creating the typical pore shapes between the extruded lines. The fracture toughness of the printed samples displayed usual values for plastic forming of alumina [29]. Since the Young's moduli and the hardness were consistent with usual values for alumina, improving the density should widely increase the mechanical properties of the parts.

For this specific binder, if the binder required melting to incorporate the ceramic powder, such as in the V2 and V3 filaments, then adding the ceramic in the form of a deagglomerated and dispersed suspension improves the rheology and the mechanical properties of the filament. Preparing a feedstock without melting the binder, as for the V1 feedstock, may considerably reduce the processing time but it would only be possible if the polymer binder is added in the form of powder instead of pellets and if a component of the binder builds strong agglomerates.

Author Contributions: Conceptualization, T.H.; methodology, T.H.; software, T.H.; validation, T.H.; formal analysis, T.H.; investigation, T.H.; data curation, T.H.; writing—original draft preparation, T.H.; writing—review and editing, T.H. and F.K.; visualization, T.H.; supervision, F.K.; project administration, T.H. All authors have read and agreed to the published version of the manuscript.

Funding: This research received no external funding.

Institutional Review Board Statement: Not applicable.

Informed Consent Statement: Not applicable.

Data Availability Statement: All relevant data to follow the content are shared in the paper.

Conflicts of Interest: The authors declare no conflict of interest.

References

1. Lakhdar, Y.; Tuck, C.; Binner, J.; Terry, A.; Goodridge, R. Additive manufacturing of advanced ceramic materials. *Prog. Mater. Sci.* **2021**, *116*, 1000736. [CrossRef]
2. Sathies, T.; Senthil, P.; Anoop, M. A review on advancements in applications of fused deposition modelling process. *Rapid Prototyp. J.* **2020**, *26*, 669–687.
3. Singh, S.; Singh, G.; Prakash, C.; Ramakrishna, S. Current status and future directions of fused filament fabrication. *J. Manuf. Process.* **2020**, *55*, 288–306. [CrossRef]
4. Li, W.; Leu, M.C. Material Extrusion Based Ceramic Additive Manufacturing. *ASM Handb. Addit. Manuf. Process.* **2020**, *24*, 97–111.
5. Dai, C.; Qi, G.; Rangarajan, S.; Wu, S.; Langrana, N.; Safari, A.; Danforth, S.C. High Quality, Fully Dense Ceramic Components Manufactured Using Fused Deposition of Ceramics (FDC). In Proceedings of the 1997 International Solid Freeform Fabrication Symposium, Austin, TX, USA, 11–13 August 1997.
6. Coble, R.L.; Kingery, W.D. Effect of Porosity on Physical Properties of Sintered Alumina. *J. Am. Ceram. Soc.* **1956**, *39*, 377–385. [CrossRef]
7. Frischholz, P. *Breviary Technical Ceramics*; Verband der Keramischen Industrie e.V.; Fahner Verlag: Lauf an der Pegnitz, Germany, 2004.
8. Gonzalea-Gutierrez, J.; Cano, S.; Schuschnigg, S.; Kukla, C.; Sapkota, J.; Holzer, C. Additive Manufacturing of Mettalic and Ceramic Components by the Material Extrusion of Highly-Filled Polymers: A Review and Future Perspectives. *Materials* **2018**, *11*, 840. [CrossRef]
9. Gerl, S.; Seiler, A.; Nikolay, D.; Kollenberg, W. Aufbereitung von Niederdruckspritzgießmassen mittels Eirich Intensivmischer. *Keram. Z.* **2009**, *61*, 286–293.
10. Conzelmann, N.; Gorjan, L.; Sarraf, F.; Poulikakos, L.; Partl, M.; Müller, C.; Clemens, F. Manufacturing complex Al_2O_3 ceramic structures using consumer-grade fused deposition modelling printers. *Rapid Prototyp. J.* **2020**, *26*, 1035–1048. [CrossRef]
11. Bricout, J.; Gelin, J.-C.; Ablitzer, C.; Matheron, P.; Brothier, M. Influence of powder characteristics on the behaviour of PIM feedstock. *Chem. Eng. Res. Des.* **2013**, *91*, 2484–2490. [CrossRef]
12. Gorjan, L.; Galusca, C.; Sami, M.; Sebastian, T.; Clemens, F. Effect of stearic acid on rheological properties and printability of ethylene vinyl acetate based feedstocks for fused filament fabrication of alumina. *Addit. Manuf.* **2020**, *36*, 101391. [CrossRef]

13. Cano, S.C. Development of Ceramic Feedstocks for Fused Filament Fabrication. Ph.D. Thesis, Montan Universität, Loeben, Austria, 2020.
14. Sommer, F.; Walcher, H.; Kern, F.; Maetzig, M.; Gadow, R. Influence of feedstock preparation on ceramic injection molding and microstructural features of zirconia toughened alumina. *J. Eur. Ceram. Soc.* **2014**, *34*, 745–751. [CrossRef]
15. Trunec, M.; Dobšák, P.; Cihlář, J. Effect of powder treatment on injection moulded zirconia ceramics. *J. Eur. Ceram. Soc.* **2000**, *20*, 859–866. [CrossRef]
16. Nötzel, D.; Hanemann, T. New Feedstock System for Fused Filament Fabrication of Sintered Alumina Parts. *Materials* **2020**, *13*, 4461. [CrossRef]
17. Esslinger, S.; Grebhardt, A.; Jaeger, J.; Kern, F.; Killinger, A.; Bonten, C.; Gadow, R. Additive Manufacturing of ß-Tricalcium Phosphate Components via Fused Deposition of Ceramics (FDC). *Materials* **2021**, *14*, 156. [CrossRef]
18. Sommer, F. *Spritzgießen von Mischkeramiken zur Herstellung Endkonturnaher Schneiden für die Zerspanung von Holz-und Holzwerkstoffen*; Shaker Verlag: Aachen, Germany, 2015.
19. *ISO 527:2012*; Standard—Plastics—Determination of Tensile Properties. ISO: Geneva, Switzerland, 2012.
20. Chudoba, T. Measurement of Hardness and Young's Modulus by Nanoindentation. In *Nanostructured Coatings. Nanostructure Science and Technology*; Springer: New York, NY, USA, 2006; pp. 216–260.
21. Szutkowska, M. Fracture toughness of advanced alumina ceramics and alumina matrix composites used for cutting tool edges. *J. Achiev. Mater. Manuf. Eng.* **2012**, *54*, 202–210.
22. Song, J.H.; Evans, J.R.G. The effect of undispersed agglomerates on the relative viscosity of ceramic moulding suspensions. *J. Mater. Sci. Lett.* **1994**, *13*, 1642–1644. [CrossRef]
23. Go, J.; Schiffres, S.N.; Stevens, A.G.; Hart, A.J. Rate limits of additive manufacturing by fused filament fabrication and guidelines for high-throughput system design. *Addit. Manuf.* **2017**, *16*, 1–11. [CrossRef]
24. Llorca, J. Deformation and Damage in Particle-Reinforced Composites: Experiments and Models. In *Mechanics of Microstructured Materials. International Centre for Mechanical Sciences*; Springer: Vienna, Austria, 2004; Volume 464, pp. 87–124.
25. Nakonieczny, D.; Kern, F.; Dufner, L.; Antonowicz, M.; Matus, K. Alumina and Zirconia-Reinforced Polyamide PA-12 Composites for Biomedical Additive Manufacturing. *Materials* **2021**, *14*, 6201. [CrossRef] [PubMed]
26. Cano, S.; Gooneie, A.; Kukla, C.; Rieß, G.; Holzer, C.; Gonzalez-Gutierrez, J. Modification of Interfacial Interactions in Ceramic-Polymer Nanocomposites by Grafting: Morphology and Properties for Powder Injection Molding and Additive Manufacturing. *Appl. Sci.* **2020**, *10*, 1471. [CrossRef]
27. Silva, L.; Tognana, S.; Salgueiro, W. Study of the water absorption and its influence on the Young's modulus in a commercial polyamide. *Polym. Test.* **2013**, *32*, 158–164. [CrossRef]
28. Mackay, M.E. The importance of rheological behavior in the additive manufacturing technique material extrusion. *J. Rheol.* **2018**, *62*, 1549. [CrossRef]
29. Ninz, P. *Dotierte Aluminiumoxid Substrate und Deren Herstellungsprozessketten für die Selektive Laserinduzierte Metallisierung*; Shaker Verlag: Düren, Germany, 2022.